

KREEP cumulates in the western lunar highlands: Ion and electron microprobe study of alkali-suite anorthosites and norites from Apollo 12 and 14

JOHN W. SHERVAIS* AND JAMES J. MCGEE

Department of Geological Sciences, University of South Carolina, Columbia, South Carolina 29208, U.S.A.

ABSTRACT

Alkali suite anorthosites and norites are the second most common plutonic rock association in the western lunar highlands (after the magnesian suite), but their origin poses an enigma for most petrologic models of lunar crustal evolution. Some models suggest that the alkali and magnesian suites formed from distinct, unrelated parental magmas, whereas other models propose that both suites formed from the same parental magma. The contrast in major element chemistry of the cumulus phases in each suite is difficult to reconcile with their similar incompatible element chemistry.

We present herein a detailed ion microprobe (SIMS) and electron microprobe study of seven alkali suite rocks. Our data show that most alkali suite anorthosites preserve major and trace element characteristics acquired during their formation as igneous cumulate rocks, and that these characteristics can be used to reconstruct the parental-magma composition. The data indicate that cumulates of the alkali suite crystallized from magmas with rare-earth element (REE) contents $\sim 0.6\text{--}2.0\times$ high-K KREEP, and small but consistently positive Eu anomalies ($\text{Eu}/\text{Eu}^* \sim 2$) relative to KREEP. Snyder and others (1995a) have proposed that the alkali suite parental magma is similar to Apollo 15 pristine KREEP basalt. Our model suggests that the major element composition of cumulus plagioclase in most alkali suite rocks is too sodic for the calculated crystal line-of-descent of pristine KREEP basalt, and that assimilation of pre-existing calcic anorthosite is required. This conclusion is supported by the REE patterns of the alkali-suite parental magma determined here.

We propose that alkali suite anorthosites formed as flotation cumulates in KREEPy plutons that may have formed norites as complementary bottom cumulates. The alkali flotation cumulates reflect fractional crystallization of their parental pluton, local equilibrium crystallization, assimilation of plagioclase-rich roof rock, and episodic magma-mixing during convective overturn of the crystallizing magma bodies. Texturally pristine alkali anorthosites exhibit petrographic characteristics that are consistent with their origin as cumulates in a KREEPy pluton, including abundant modal plagioclase, post-cumulus pyroxenes (both augite and pigeonite) that generally lack exsolution lamellae and that have equilibration temperatures of $950\text{--}1100^\circ\text{C}$, relict igneous textures and, in some cases, igneous lamination. The lack of cumulus mafic phases in rocks that should be pyroxene-saturated suggests separation of the plagioclase by flotation, not sinking. Assimilation of plagioclase from older, anorthositic highlands crust is indicated by the high Eu contents of the cumulates and by the positive Eu anomalies in their calculated parental melts relative to high-K KREEP. Mixing of the evolved alkali-suite parental magma with primitive melt occurred episodically, as shown by reverse zoning profiles in some cumulus plagioclase. Injection of this primitive, hot magma into the crystallizing pluton may have induced convective overturn of the magma chamber.

INTRODUCTION

“KREEP” is a globally distributed chemical component that permeates a wide variety of lunar rocks, but which is never found in its pristine, unadulterated state (Meyer et al. 1971). An acronym that reflects its characteristic high concentrations of potassium, rare earth elements, and phosphorus, KREEP is thought to represent the last magmatic dregs of the lunar magma ocean, termed “urKREEP” (“original KREEP”) by Warren and Wasson (1980). Other products of this moon-wide melting event include the anorthositic lunar crust (thought to have resulted

from the flotation of cumulus plagioclase) and the ultramafic lunar mantle (thought to have formed by the sinking of mafic phases). Recent work on the petrologic and chemical evolution of the moon’s crust has shown that this residual magmatic component had a profound impact on all subsequent igneous activity (e.g., Warren 1988; Shervais 1989; Snyder et al. 1992; Papike 1996).

One of the most intriguing assemblages of lunar plutonic igneous rocks is the “alkali suite,” which post-dates crystallization of the lunar magma ocean (Snyder et al. 1995a). The alkali suite is characterized by plagioclase compositions that are relatively sodic by lunar standards ($\sim \text{An}_{70}$ to $\sim \text{An}_{90}$), by relatively evolved, Fe-rich mafic phases (olivine Fo_{67} to Fo_{74} ;

*E-mail: shervais@geol.sc.edu

pyroxene $mg' [=100 * Mg / (Mg + Fe) \text{ molar}]$ of 51–78), and by accessory phases that may include silica, potassium feldspar, fayalite, ilmenite, and phosphates (typically whitlockite). In contrast, the more common magnesian suite is characterized by refractory mineral assemblages that include olivine (FO_{78} to FO_{89}), calcic plagioclase (AN_{87} to AN_{97}), diopside and enstatite (mg' of 88–90), and pink spinel; pigeonite (mg' 68–80) is found only in the more evolved magnesian norites (Fig. 1). Both of these post-magma ocean plutonic suites intruded the older, ferroan anorthositic crust in the period between about ~4.4 and ~3.9 Ga (Snyder et al. 1995a, 1995b).

Because plutonic rocks of the alkali suite are found only as clasts in polymict lunar breccias, or as reworked clasts in regolith breccias or soil, the amount of sample available (commonly <100 mg) is too small to obtain representative whole-rock analyses (e.g., Shervais et al. 1990). Furthermore, even if representative whole-rock data are available, it is not possible to calculate directly the composition of parental magmas from whole-rock analyses of cumulate igneous rocks—the number of unknowns always exceeds the number of simultaneous equations that can be written to describe the system (note that these

equations can be solved if the amount of trapped liquid can be determined independently).

This problem can be overcome by analyzing the trace-element composition of primary cumulus phases using secondary ion mass spectrometry (SIMS) and “inverting” the data (using mineral/melt distribution coefficients) to estimate the trace-element composition of the cumulate’s parental magma. This approach eliminates the need for representative whole-rock analyses, and can be applied to texturally pristine samples known only in thin section, as well as to clasts that have been extracted from their matrix. The SIMS approach also allows us to monitor the evolution of the trapped intercumulus melt by analyzing post-cumulus grains and the rims of cumulus phases.

The application of SIMS analysis to lunar samples was rare until recently. Early studies of lunar samples focused largely on accessory minerals (e.g., Crozaz and Zinner 1985), basaltic glasses in lunar soils (Papike et al. 1990; Shearer et al. 1990; Galbreath et al. 1990), or supposed immiscible glasses (Snyder et al. 1993). It has only been in the last five years that systematic SIMS studies have attacked the problem of cumulate rock petrogenesis in the lunar highlands (Papike et al. 1994, 1996; Papike 1996; Shervais 1994, 1996; Shervais and Stuart 1995; Snyder et al. 1994; Shervais and McGee 1997a, 1998a; Jolliff et al. 1993).

Almost all previous studies that applied SIMS analysis to the evolution of lunar highlands crust have focused on magnesian suite rocks (Papike et al. 1994, 1996; Papike 1996; Snyder et al. 1994; Shervais and McGee 1998a). Preliminary SIMS results on alkali suite rocks have been reported by Shervais (1994), Shervais and Stuart (1995), and Snyder et al. (1994). We report here the first complete SIMS investigation of alkali suite anorthosites and norites. All of the samples studied here are characterized by relatively sodic plagioclase compositions (AN_{75} to AN_{88}) and by intermediate-Mg pyroxene (mg' 40 to 70; Fig. 1). These rocks represent cumulates from lunar parental magmas that are evolved compared with parental melts of the magnesian suite. An important difference between this study and the earlier studies is that we do not present “average data” for individual samples (e.g., Papike et al. 1994, 1996); rather, we present individual spot analyses so that we may compare variations within individual samples, between cores and rims in the same grain, and between different phases. One advantage of this approach is that we can assess the effects of subsolidus reequilibration directly and assess whether inversion of the trace element data can be used to obtain equilibrium melt compositions.

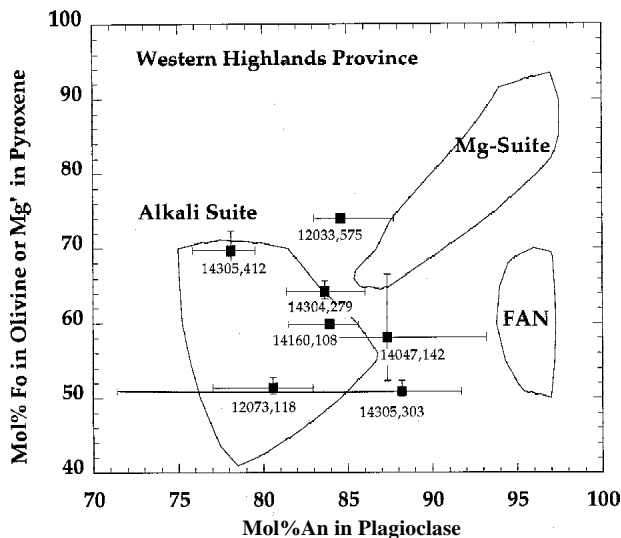


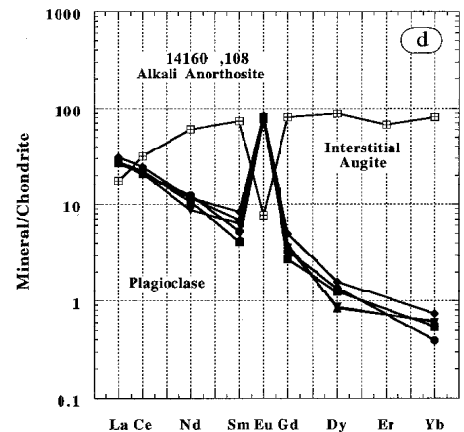
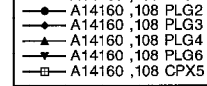
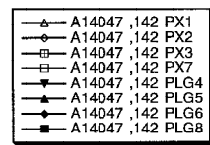
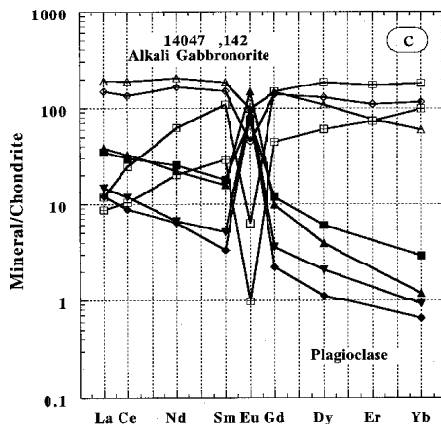
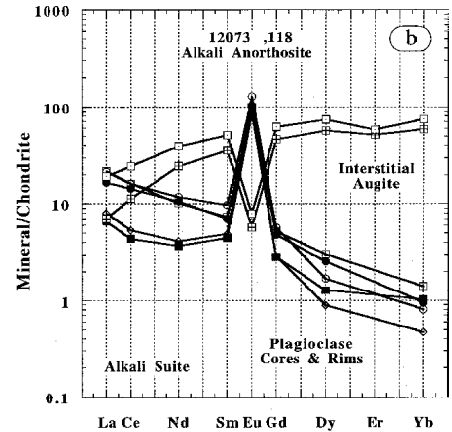
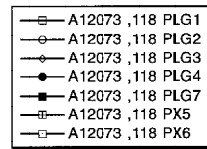
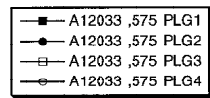
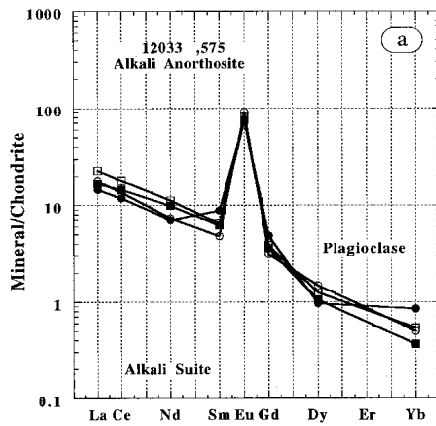
FIGURE 1. Pyroxene Mg'-Plagioclase An diagram for alkali suite lunar rocks from the western lunar highlands, showing average mineral compositions of samples used in this study, with bars showing the range in composition of each phase.

TABLE 1. Samples of alkali suite anorthosites and norites analyzed by SIMS for trace element concentrations in pyroxene and/or plagioclase (Pristinity index of Warren 1993)

Generic	Specific subsample	Parent or other subsample	Rock type	pristine index*	SIMS anal.	Primary reference
12033	,575	,425 ,501	Anorthosite	8.0	4	Warren et al. 1990
12073	,118	,120 ,122	Anorthosite	6.6	7	Warren et al. 1981; Warren and Wasson 1980
14047	,142	,112 ,113	Anorthositic Norite	6.9	8	Warren et al. 1983a
14160	,108	,88 ,105 ,106	Anorthosite	6.5	6	Warren and Wasson 1980
14304	,279	,86 ,87 "g"	Norite	7.0	9	Goodrich et al. 1986
14305	,303	,283	Anorthosite	6.8	2	Warren et al. 1983b
14305	,412	,400	Anorthosite	6.2	11	Shervais et al. 1984

TABLE 2. Average mineral compositions

	A12033,575		A12073,118		A14047,142			A14160,108			A14304,279			A14305,303		A14305,412	
	Plagio- class	Augite	Plagio- class	Augite	Plagio- class	Augite	Hyper- sthene	Pigeo- nite	Plagio- class	Augite	Plagio- class	Augite	Hyper- sthene	Plagio- class	Pigeo- nite	Plagio- class	Augite
SiO ₂	47.44	52.15	48.52	50.59	45.81	51.94	52.67	51.12	47.30	50.24	47.59	52.85	52.21	45.73	50.96	49.28	51.90
TiO ₂		0.46		0.50	0.03	0.64	0.50	0.47	0.03	0.57		0.75	0.53		0.65		0.87
Al ₂ O ₃	33.82	0.75	32.68	0.56	34.54	1.08	0.79	0.59	33.63	0.71	33.26	1.06	0.86	34.77	0.60	31.59	0.94
Cr ₂ O ₃		0.21		0.23	0.00	0.28	0.30	0.19	0.00	0.19		0.41	0.34		0.13		0.21
MgO	0.05	14.58	0.03	10.38	0.04	13.59	21.68	16.57	0.05	12.62	0.05	14.71	22.16		15.76	0.09	14.74
CaO	16.77	21.75	16.00	19.15	17.55	18.96	1.87	5.07	16.70	18.38	16.64	22.07	1.75	18.15	4.99	15.44	18.87
MnO		0.18		0.26	0.00	0.23	0.30	0.42	0.00	0.26		0.13	0.35		0.46	0.00	0.27
FeO	0.13	9.14	0.15	17.49	0.11	13.41	22.43	25.47	0.13	15.09	0.10	8.02	21.90	0.16	27.04	0.15	11.67
BaO		0.04		0.07		0.06				0.06		0.01					0.07
Na ₂ O	1.55	0.08	1.99	0.09	1.31	0.12	0.01	0.04	1.66	0.09	1.66	0.14	0.02	1.25	0.03	2.17	0.12
K ₂ O	0.21	0.00	0.22	0.00	0.15	0.00	0.00	0.00	0.18	0.00	0.19	0.00	0.01	0.17	0.00	0.38	0.00
Total	100.00	99.30	99.66	99.26	99.59	100.27	100.56	99.95	99.74	98.15	99.52	100.14	100.12	100.23	100.62	99.17	99.59
An	84.6		80.6		87.4				83.9		83.7			88.0		77.9	
Mg'		74.0		51.4		64.4	63.3	53.7		59.8		76.57	64.3		50.9		69.2
Formula proportions of cations based on eight (plagioclase) and six (pyroxene) O atoms																	
Si	2.175	1.962	2.228	1.969	2.118	1.957	1.960	1.966	2.176	1.954	2.191	1.961	1.950	2.104	1.960	2.271	1.955
Ti		0.013		0.015		0.018	0.014	0.014		0.017		0.021	0.015	0.000	0.019		0.025
Al	1.829	0.033	1.770	0.026	1.884	0.048	0.035	0.027	1.825	0.032	1.807	0.046	0.038	1.887	0.027	1.717	0.042
Cr		0.006		0.007		0.008	0.009	0.006		0.006		0.012	0.010	0.000	0.004		0.006
Mg	0.003	0.818	0.002	0.602	0.003	0.764	1.203	0.949	0.003	0.732	0.004	0.813	1.233	0.000	0.903	0.006	0.827
Ca	0.824	0.877	0.787	0.799	0.869	0.766	0.074	0.209	0.823	0.766	0.821	0.877	0.070	0.895	0.206	0.762	0.761
Mn		0.006		0.008		0.007	0.010	0.014		0.008		0.004	0.011	0.000	0.015		0.008
Fe	0.005	0.288	0.006	0.570	0.004	0.423	0.698	0.819	0.005	0.491	0.004	0.249	0.684	0.006	0.870	0.006	0.368
Ba	0.001		0.001		0.001				0.001		0.000						0.001
Na	0.138	0.006	0.177	0.007	0.117	0.009	0.001	0.003	0.148	0.007	0.148	0.010	0.001	0.112	0.002	0.194	0.009
K	0.012	0.000	0.013	0.000	0.009	0.000	0.000	0.000	0.011	0.000	0.011	0.000	0.000	0.010	0.000	0.022	0.000
SUM	4.987	4.008	4.984	4.003	5.005	4.001	4.004	4.006	4.992	4.013	4.987	3.994	4.012	5.014	4.007	4.980	4.001



TECHNIQUES

Seven samples were chosen for this study: five anorthosites, one anorthositic norite, and one norite. These samples were chosen because all have been studied previously (Table 1), and most have corresponding bulk INAA analyses. In addition, all of these samples are considered to be "probably pristine" (that is, monomict igneous rocks, not impact melts) using the pristinity index of Warren (1993). Each sample was re-evaluated petrographically, and new major-element mineral-chemical data were obtained by electron microprobe analysis to confirm published data, to assess the extent of compositional zoning, and to document the composition of each ion probe analysis. Average major-element mineral compositions for each sample are reported in Table 2.

Quantitative electron microprobe analyses of major and minor elements were obtained with a Cameca SX50 four-wavelength-spectrometer automated electron microprobe. The samples were examined optically and by secondary and backscattered electron imagery using the electron microprobe. Analyses were made at 20 kV accelerating voltage, 30 nA probe current, and counting times of 20–100 s, using natural and synthetic mineral standards. Analyses were corrected for instrumental drift and deadtime, and electron beam/matrix effects using the "PAP" correction procedures provided with the

Cameca microprobe automation system (Pouchou and Pichoir 1991). Relative accuracy of the analyses, based upon comparison between measured and published compositions of the standards, is ~1–2% for oxide concentrations >1 wt% and ~10% for oxide concentrations <1 wt%.

Ion microprobe analyses were carried out on the Cameca IMS 3f secondary ion mass spectrometer at the Woods Hole Oceanographic Institute/MIT SIMS Facility, under the direction of Nobu Shimizu. A primary beam of O^- ions with an accelerating potential of ~8 KeV and a beam current of ~10 nA was focused to a spot size of 15–25 μm in diameter. Secondary ion intensities for $^{30}\text{Si}^+$, $^{139}\text{La}^+$, $^{140}\text{Ce}^+$, $^{146}\text{Nd}^+$, $^{147}\text{Sm}^+$, $^{153}\text{Eu}^+$, $^{163}\text{Dy}^+$, $^{167}\text{Er}^+$, and $^{174}\text{Yb}^+$ were measured using kinetic energy filtering, which lowers molecular ion interferences from the secondary ion mass spectra by reducing the secondary ion accelerating voltage (Shimizu and Hart 1982; Shimizu 1978, 1997). The secondary accelerating voltage was 4500 volts, with an HV sample offset of -60 volts in the secondary beam column. Secondary ions were detected by an electron multiplier in pulse-counting mode. Secondary intensities of the rare earth elements (REE) were normalized to $^{30}\text{Si}^+$, and referenced to working curves produced from a well-calibrated set of pyroxene standards (Roden and Shimizu 1993; Shimizu 1997). Plagioclase working curves were developed using the Moore

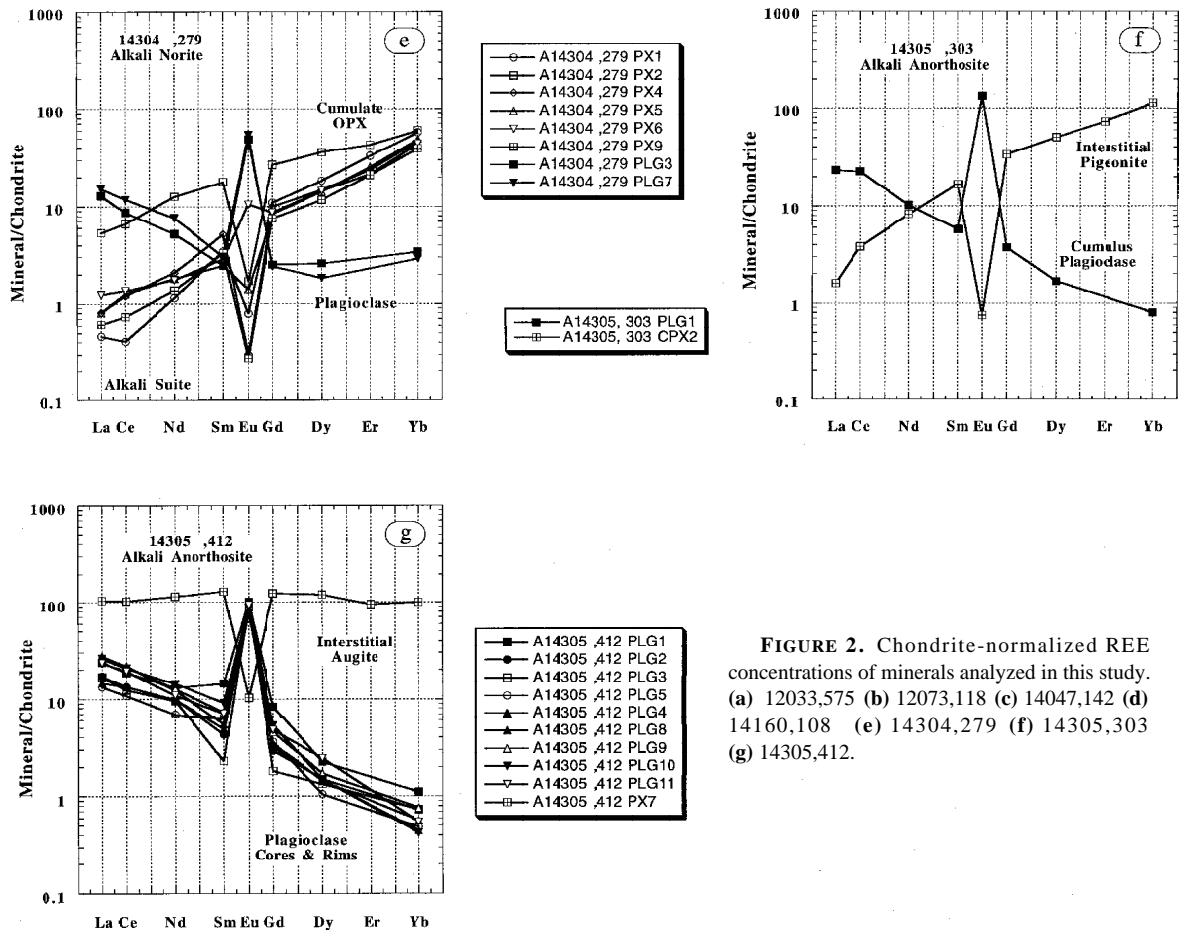


FIGURE 2. Chondrite-normalized REE concentrations of minerals analyzed in this study. (a) 12033,575 (b) 12073,118 (c) 14047,142 (d) 14160,108 (e) 14304,279 (f) 14305,303 (g) 14305,412.

TABLE 3. Major and trace element composition of SIMS spots

	A12033,575					A12073,118					
	PlagA Core Spot 1	PlagA Rim Spot 2	PlagB Core Spot 3	PlagC Core Spot 4	Plag Core Spot 1	Plag Core Spot 2	Plag Rim Spot 3	Plag Core Spot 4	Plag Rim Spot 7	Augite Post Spot 5	Augite Post Spot 6
SiO ₂	47.641	47.46	47.02	47.98	48.39	48.632	48.77	48.34	47.63	50.30	50.72
TiO ₂										0.45	0.41
Al ₂ O ₃	33.826	34.12	33.90	34.07	33.15	32.388	32.48	32.43	33.12	0.49	0.52
Cr ₂ O ₃										0.24	0.21
MgO	0.052	0.04	0.05	0.05	0.03	0.031	0.04	0.03	0.04	10.57	10.39
CaO	16.757	16.85	16.87	16.79	16.14	15.857	16.10	15.98	16.38	19.71	19.31
MnO										0.26	0.25
FeO	0.046	0.08	0.16	0.10	0.13	0.157	0.17	0.15	0.16	16.85	17.61
BaO	0.041	0.03	0.00	0.00	0.15	0.028	0.00	0.15	0.07		
Na ₂ O	1.664	1.62	1.42	1.65	1.99	1.99	1.96	2.13	1.90	0.09	0.10
K ₂ O	0.164	0.19	0.28	0.16	0.21	0.225	0.21	0.21	0.19	0.01	0.00
Total	100.191	100.38	99.69	100.78	100.18	99.308	99.73	99.42	99.49	98.97	99.53
An	83.9	84.2	85.4	84.1	80.8	80.4	80.9	79.6	81.7		
Mg' ppm										52.8	51.2
La	5.75	5.00	7.72	6.14	7.40	7.38	2.72	5.69	2.22	2.37	6.60
Ce	13.34	10.83	16.48	12.40	14.78	14.61	4.84	13.08	3.95	10.25	22.29
Nd	5.77	4.07	6.53	4.25	5.87	6.84	2.40	6.10	2.15	14.27	22.64
Sm	1.20	1.71	1.25	0.94	1.43	1.89	0.95	1.36	0.87	6.94	9.94
Eu	5.53	5.31	6.09	6.67	7.31	9.32	7.41	7.52	6.26	0.42	0.58
Gd*	0.75	0.99	0.81	0.68	1.15	1.19	0.60	1.05	0.61	11.51	15.42
Dy	0.30	0.27	0.36	0.43	0.87	0.48	0.26	0.73	0.36	16.08	20.90
Er										10.05	11.29
Yb	0.073	0.169	0.107	0.100	0.281	0.162	0.095	0.191	0.206	11.71	14.79

Note: Major and minor elements in weight percent oxide, REE in parts per million. An = mol% anorthite in plagioclase ($100 \times \text{Ca}/[\text{Ca}+\text{Na}+\text{K}]$); Mg' = $100 \times \text{Mg}/[\text{Mg}+\text{Fe}]$ molar, in mafic phases; Gd* = Gd interpolated from adjacent REE.

TABLE 3.—Continued

	A14304,279						A14305,303			
	Plag Core Spot 3	Plag Core Spot 7	Lo-CaPyx Core A Spot 1	Lo-CaPyx Rim A Spot 2	Lo-CaPyx Core B Spot 4	Lo-CaPyx Core B Spot 5	Lo-CaPyx Rim B Spot 6	Lo-Ca Pyx Core C Spot 9	Plag Core Spot	Pigeonite Post Spot
SiO ₂	47.77	47.22	51.56	52.29	52.61	52.34	52.01	52.57	44.92	50.55
TiO ₂			0.37	0.37	0.71	0.79	0.45	0.38		0.58
Al ₂ O ₃	33.15	33.84	0.86	0.86	0.96	1.02	1.02	0.91		35.12
0.49 Cr ₂ O ₃			0.32	0.31	0.36	0.42	0.37	0.35		
0.11 MgO	0.03	0.03	22.23	23.04	21.86	22.10	22.15	21.90		15.68
CaO	16.49	17.14	1.53	0.97	2.34	2.08	2.00	2.22	18.64	4.26
MnO			0.32	0.35	0.35	0.36	0.32	0.35		0.49
FeO	0.11	0.04	22.34	21.45	21.46	21.80	21.51	21.67	0.149	27.62
BaO	0.00	0.02								
Na ₂ O	1.79	1.47	0.02	0.03	0.01	0.02	0.00	0.05	1.07	0.02
K ₂ O	0.14	0.19	0.00	0.10	0.00	0.00	0.00	0.00	0.130	0.00
Total	99.48	99.93	99.55	99.76	100.65	100.92	99.82	100.39	100.03	99.80
An	82.9	85.6							89.9	
Mg' ppm			63.9	65.7	64.5	64.4	64.7	64.3		50.3
La	4.41	5.21	0.16	1.81	0.28	0.28	0.41	0.21	7.90	0.54
Ce	7.88	10.88	0.37	6.05	1.09	1.14	1.23	0.67	20.59	3.48
Nd	3.02	4.43	0.67	7.37	1.20	1.04	1.02	0.79	5.92	4.78
Sm	0.48	0.59	0.68	3.50	1.01	0.48	0.56	0.64	1.13	3.28
Eu	3.55	3.95	0.06	0.12	0.02	0.10	0.77	0.02	9.70	0.06
Gd*	0.61	0.55	2.98	6.86	2.63	2.28	2.36	2.00	0.80	8.84
Dy	0.74	0.52	5.29	10.21	4.26	4.08	4.16	3.35	0.48	14.41
Er			6.40	8.36	4.67	4.97	4.24	4.15		14.10
Yb	0.688	0.582	11.49	11.95	9.37	9.75	8.73	7.86	0.160	22.60

County achondrite and the adjusted plagioclase REE concentrations of Papike et al. (1996). Counts were referenced to a monitor (KL-2) measured at the beginning of each run. Analytical precision for the REE is 5–10% in pyroxene (Roden and Shimizu 1993) whereas in plagioclase, precision is 5–10% for the LREE and Eu and no better than 15% for the HREE

because of their low concentrations (N. Shimizu, personal communication 1996).

Eight REE (La, Ce, Nd, Sm, Eu, Dy, Er, Yb) were analyzed with the ion microprobe; Gd is interpolated. In brecciated samples, only the cores of large relict cumulus grains were analyzed. Texturally pristine samples with well-preserved relict

TABLE 3.—*Extended*

	A14047,142								A14160,108					
	Plag Core Spot 4	Plag Core Spot 5	Plag Core Spot 6	Plag Core Spot 8	Augite Post Spot 7	Pigeonite Post Spot 1	Pigeonite Post Spot 2	Pigeonite Post Spot 3	Plag A Core Spot 1	Plag A Rim Spot 2	Plag B Core Spot 3	Plag B Rim Spot 4	Plag C Core Spot 6	Augite Post Spot 5
SiO ₂	47.54	47.47	46.77	43.91	51.97	51.08	50.79	51.29	47.22	46.87	47.78	45.84	47.03	50.52
TiO ₂	0.03	0.02	0.03	0.04	0.66	0.43	0.47	0.48	0.03	0.02		0.03	0.02	0.55
Al ₂ O ₃	33.80	33.93	34.41	35.74	1.00	0.53	0.60	0.52	33.85	33.97	33.17	33.84	34.03	0.71
Cr ₂ O ₃	0.00	0.01	0.00	0.00	0.27	0.20	0.20	0.20	0.00	0.00		0.00	0.00	0.18
MgO	0.04	0.06	0.05	0.02	13.67	16.84	16.56	16.82	0.05	0.06	0.05	0.06	0.04	12.74
CaO	16.41	16.44	17.14	18.71	19.09	4.58	4.95	4.17	16.66	16.58	16.71	16.91	16.65	18.18
MnO	0.01	0.00	0.02	0.00	0.27	0.43	0.41	0.45	0.00	0.01		0.01	0.03	0.26
FeO	0.14	0.11	0.07	0.07	13.09	25.64	25.45	26.23	0.14	0.13	0.14	0.15	0.13	15.37
BaO										0.11				
Na ₂ O	1.86	1.76	1.54	0.81	0.13	0.05	0.05	0.01	1.69	1.72	1.64	1.64	1.67	0.09
K ₂ O	0.25	0.20	0.17	0.06	0.01	0.00	0.00	0.01	0.21	0.17	0.17	0.18	0.17	0.01
Total	100.09	99.99	100.21	99.36	100.16	99.77	99.47	100.17	99.85	99.52	99.77	98.65	99.77	98.60
An	81.7	82.8	85.2	92.5					83.5	83.3	84.1	84.2	83.8	
Mg' ppm					65.0	53.9	53.7	53.3						59.6
La	5.00	13.11	4.16	11.97	4.07	65.86	50.46	2.97	9.32	9.30	10.51	9.17	8.97	5.98
Ce	10.83	29.81	7.97	27.13	22.50	174.37	122.50	9.56	20.28	18.87	22.49	18.81	19.17	28.85
Nd	3.83	12.78	3.68	14.79	36.33	119.90	95.62	11.77	6.14	7.20	6.77	6.74	5.02	34.93
Sm	0.99	3.06	0.65	3.49	21.25	36.41	29.31	5.67	0.81	1.02	1.63	1.34	1.22	14.38
Eu	6.98	10.90	6.09	5.46	0.46	7.18	3.31	0.07	5.62	5.98	6.17	5.74	5.95	0.56
Gd*	0.80	2.09	0.49	2.60	37.38	33.76	33.07	11.47	0.58	0.70	1.04	0.79	0.73	19.83
Dy	0.60	1.13	0.32	1.71	53.51	31.10	36.82	17.26	0.35	0.39	0.45	0.24	0.25	25.28
Er					34.04	15.00	21.38	14.38						13.07
Yb	0.184	0.238	0.133	0.590	36.41	11.94	23.05	19.66	0.109	0.079	0.147	0.124	0.121	16.171

TABLE 3.—*Extended*

	A14305,412										
	Plag A Core Spot 1	Plag A Half Spot 2	Plag A Rim Spot 3	Plag A Rim Spot 5	Plag B Core Spot 4	Plag C Core Spot 8	Plag C Rim Spot 9	Plag D Core Spot 10	Plag D Rim Spot 11	Augite Post Spot 7	
SiO ₂	49.34	49.36	49.35	49.61	48.30	49.12	49.07	49.37	48.97	52.28	
TiO ₂										0.82	
Al ₂ O ₃	32.42	32.20	32.24	32.12	32.61	31.87	31.99	31.84	32.08	0.86	
Cr ₂ O ₃										0.18	
MgO	0.09	0.09	0.10	0.11	0.10	0.08	0.10	0.09	0.10	15.09	
CaO	15.57	15.46	15.32	14.91	15.78	15.76	15.72	15.49	15.78	18.75	
MnO										0.27	
FeO	0.16	0.14	0.14	0.16	0.15	0.18	0.15	0.12	0.11	11.64	
BaO	0.07	0.05	0.07	0.09	0.02	0.05	0.02	0.03	0.04		
Na ₂ O	2.26	2.25	2.28	2.32	2.09	2.06	2.07	2.08	1.99	0.13	
K ₂ O	0.29	0.42	0.47	0.64	0.40	0.27	0.40	0.46	0.41	0.00	
Total	100.20	99.98	99.95	99.90	99.45	99.38	99.50	99.48	99.49	100.01	
An	77.9	77.2	76.6	75.1	78.7	79.6	78.9	78.2	79.4		
Mg' ppm										69.8	
La	8.05	5.85	5.75	4.56	4.97	9.34	8.95	8.80	7.90	35.28	
Ce	17.11	12.14	11.31	9.78	12.24	19.60	19.54	18.85	17.60	93.14	
Nd	7.59	5.74	5.56	3.99	5.72	7.11	7.38	8.34	6.29	66.62	
Sm	2.81	0.83	0.45	1.20	0.95	1.06	1.43	1.79	1.38	25.02	
Eu	7.39	6.18	6.70	6.44	5.61	6.83	6.84	6.61	6.78	0.76	
Gd*	1.73	0.63	0.41	0.75	0.69	0.74	0.96	1.10	1.04	29.44	
Dy	0.64	0.43	0.38	0.30	0.42	0.41	0.49	0.42	0.70	33.86	
Er										18.48	
Yb	0.222	0.145	0.147	0.097	0.089	0.113	0.153	0.084	0.109	20.08	

cumulate textures were analyzed in more detail to evaluate zoning in cumulus grains. Post-cumulus pyroxenes were analyzed in several samples to trace the evolution of the trapped liquid and to check for post-cumulus reequilibration. Concentration data for the REE and the major-element compositions of the analyzed spots are presented in Table 3.

RESULTS

12033,575

This clast is a nearly pure, monomineralic anorthosite described by Warren et al. (1990). Thin section ,575 consists of twinned, decussate-textured plagioclase that has been brecciated in part along grain boundaries. Its mode is ~99% plagioclase.

class ($An_{84.6}$) with ~1% augite ($Wo_{44}En_{40}$) and trace ilmenite. Relict cumulus plagioclase is up to 1.8 mm across, and the original cumulus grains were probably larger than 2 mm (Warren et al. 1990). Texturally, this rock is a plagioclase adcumulate, with <2% trapped melt component.

Four spots were analyzed on this sample with the ion microprobe, three cumulus plagioclase cores and one cumulus plagioclase rim (Table 3). All of the spots have chondrite-normalized REE abundances typical of plagioclase, with La ~20× chondrites, Yb ~0.5×, and a large positive Eu anomaly (Fig. 2a). Plagioclase rims are lower in La than are cores, but have slightly higher Yb (Table 3).

12073,118

This clast was described by Warren and Wasson (1980), with whole-rock chemistry reported by Warren et al. (1981). Thin section ,118 consists of several small fragments, some with glassy breccia matrix attached. The texture is cataclastic, but it contains several small, relict, unbrecciated grains. Warren and Wasson (1980) reported an estimated mode of ~99% plagioclase ($An_{78.6}$) and ~1% pigeonite (mg' 51). We identified ferroaugite in addition (Tables 2 and 3).

Seven spots were analyzed in this sample, five on plagioclase and two on tiny post-cumulus ferroaugites (Fig. 2b). Two of the plagioclases are broken grains that we interpret as the interiors of former cumulate grains (Plag1, Plag2), two are near the rims of relict cumulus clasts (Plag3, Plag7), and one is a relict cumulus core (Plag4). Three of these grains (Plag 1, 2, 4) have La ~20× and Yb ~0.9×; these are spots that we interpret as the cores of cumulus grains. The other two grains (Plag3, 7) have lower LREE concentrations, with La ~7×; these may represent original rims of cumulus grains (see sample 14305,400 below). The pigeonites have chondrite-normalized REE concentrations similar to augites, with La ~7–20× and Yb ~60–70× (Fig. 2b).

14047,142

This clast was described by Warren et al. (1983a). Our thin section was made from the same potted butt as the section studied by Warren (his sample ,113), but it exposes a slightly different part of the clast. Our section ,142 consists of several small fragments of anorthositic norite, some with thin selvages of glassy matrix breccia attached. All of the fragments are strongly brecciated, with an average grain size of ~0.04 mm (Warren et al. 1983a). A few relict plagioclase grains up to ~0.2 mm across are present; however, monomineralic crush zones of plagioclase occur that are up to 1.8 mm across, indicating an original cumulus grain size of ~1.5–2.0 mm. Warren et al. (1983a) reported a mode of ~84% plagioclase and ~16% pigeonite, with traces of potassium feldspar, ilmenite, and Fe-metal. We found ~84% plagioclase ($An_{87.4}$) and three distinct pyroxenes: pigeonite, augite, and hypersthene (Table 2). All of the pyroxenes are interpreted to be post-cumulus, based on their size and distribution within the sample.

Eight spots were analyzed with the ion probe: four plagioclase fragments, three post-cumulus pigeonites, and one post-cumulus augite. All four plagioclase spots are from the interi-

ors of small broken grains within large, plagioclase crush zones; we interpret these to be equivalent to mineral cores. Two of the spots are enriched in LREE (La ~40×) and two are relatively poorer in LREE (La ~15×; Fig. 2c). The post-cumulus pyroxenes include two pigeonites with high REE concentrations (La ~150–200×) and LREE-enriched patterns, and two pyroxenes (one augite, one pigeonite) with lower LREE concentrations (La ~9–12×) and LREE depleted patterns (Fig. 2c).

14160,108

This clast was described by Warren and Wasson (1980) as 14160,105. It is essentially a pure plagioclase anorthosite with a single, tiny (90 × 30 μm) augite crystal. Our thin section was made from the same potted butt as the section studied by Warren and Wasson (1980), and appears nearly identical to the photomicrograph published by them. Our section consists of a large, "U-shaped" fragment with coarse, cumulus-textured plagioclase in the center, and cataclastic-textured material on both ends. Relict grains in the coarse cumulus areas are up to ~1.2 mm across and preserve primary textural relationships. Plagioclase exhibits a small range in composition (one spot $An_{81.5}$, others $An_{82.9}$ to $An_{85.7}$; average $An_{83.9}$), consistent with an adcumulate origin and the near absence of trapped liquid.

Six spots were analyzed: three cumulus plagioclase cores, two cumulus plagioclase rims, and one post-cumulus augite. The plagioclase spots have La ~26–30× (Fig. 2d). One plagioclase core-rim pair is identical within analytical error, and one core is about 2 ppm richer in La than its corresponding rim and the other core. The augite has a typical pyroxene REE pattern, with high MREE and HREE (~80×) and low LREE (~20×; Fig. 2d).

14304,279

This norite corresponds to clast "g" of Goodrich et al. (1986), who reported only petrographic data. Snyder et al. (1995a) reported additional petrologic data for this sample, as well as whole-rock isotopic compositions for Sr and Nd. Our thin section was made from the same potted butt as the sections (,86 and ,87) studied by Goodrich et al., who reported a mode of ~75% pyroxene, ~14% plagioclase, and ~2% phosphates. The clast is relatively coarse-grained, with pyroxene oikocrysts up to 1.1 × 0.6 mm enclosing stubby plagioclase and pyroxene crystals (Goodrich et al. 1986). Plagioclase ($An_{81.7}$) forms twinned, blocky grains up to 0.6 mm across. Pyroxene is largely inverted pigeonite ($Wo_{3.7}En_{62}$), with coarse augite exsolution in some hypersthene grains and green, augitic overgrowths on others. The sample also contains brown, K-rich rhyolitic glass interstitial to the pyroxenes. In places, this glass outlines euhedral crystal terminations, showing that it is mesostasis, not an injected impact melt. The texture resembles that of a coarse mare basalt.

Eight spots were analyzed with the ion probe: two plagioclase cores, four hypersthene cores, and two hypersthene rims. The plagioclase grains are unusually high in the HREE relative to the LREE (Fig. 2e). All of the hypersthene but one are strongly depleted in LREE; the exception (PX2) is much higher in LREE than the others and may include some exsolved augite (Fig. 2e).

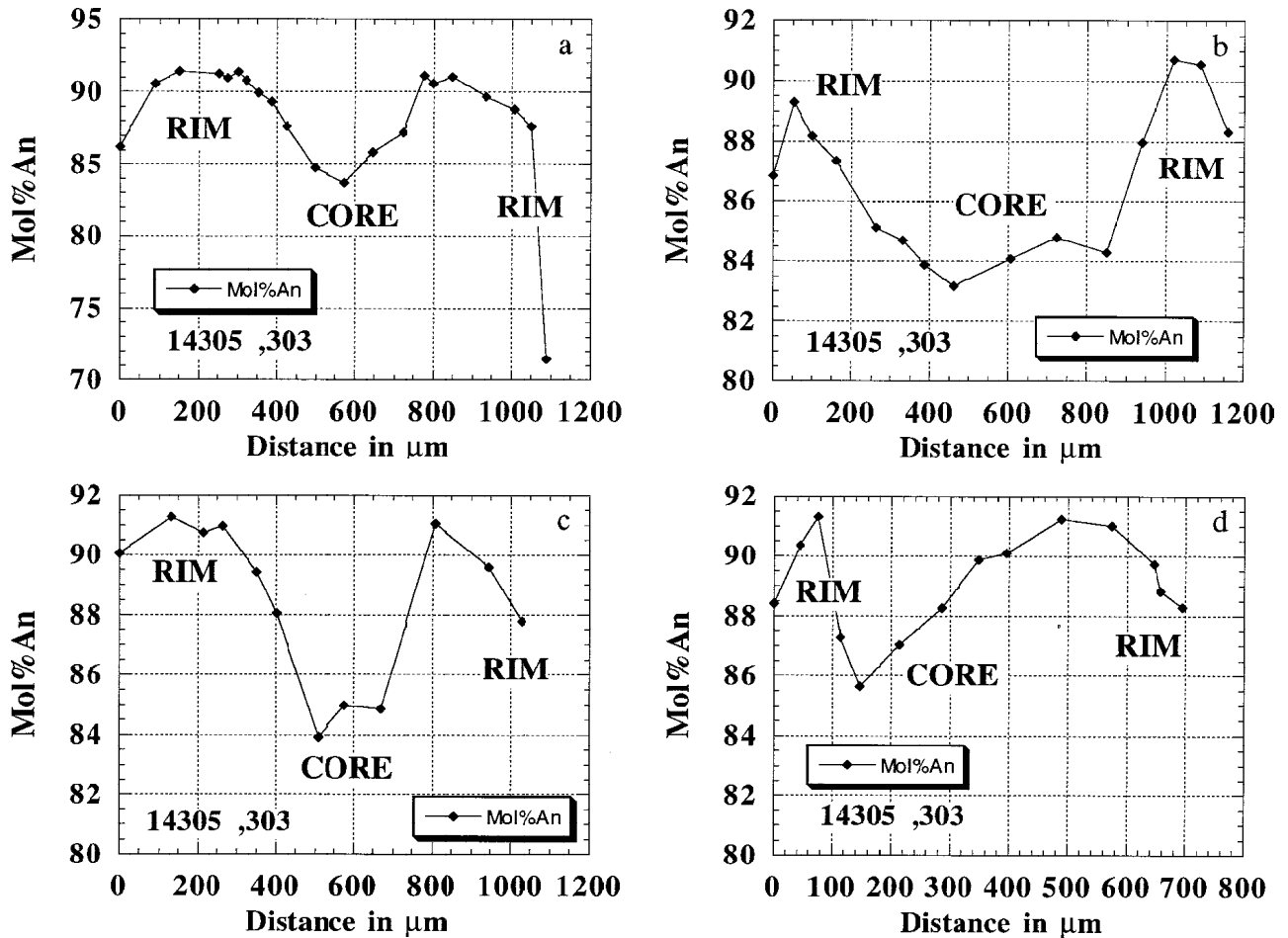


FIGURE 3. Rim-Core-Rim zoning traverses in a large cumulus plagioclase grain, 14305,303. X-axis = distance in micrometers, y-axis = mol% An in plagioclase.

14305,303

This is clast C2 of Warren et al. (1983b), which they described as an annealed monomict breccia, with unbroken plagioclase crystals up to 1.7 mm across. The mode is ~95% plagioclase, ~2.5% whitlockite, ~2% pigeonite, and ~1% augite, with trace silica, ilmenite, potassium feldspar, troilite, and Fe metal (Warren et al. 1983b). Pyroxene occurs as small post-cumulus grains between plagioclase, many in optical continuity up to 1 mm apart. Cumulus plagioclase crystals are strongly zoned, with cores ~An₈₄ to An₈₅ surrounded by thick mantles (200 to 300 μm thick) of ~An₉₁ and thin outer rims (<100 μm thick) of more sodic composition (~An₈₇ to An₈₉ typically, but as low as An₇₀; Fig. 3). These large cumulus plagioclase grains are set in a matrix of smaller plagioclase grains of ~An₈₈ composition.

Two spots were analyzed with the ion probe: one cumulus plagioclase and one post-cumulus pigeonite (Table 3). The plagioclase is LREE-enriched, with La ~23 \times , Yb ~1.5 \times , and a large positive Eu anomaly ~130 \times (Fig. 2f). The pigeonite is LREE-depleted (Fig. 2f).

14305,412

This clast (W1) was first described by Shervais et al. (1984). It consists of ~99.5% plagioclase (~An_{75.5} Or_{1.9}) and ~0.4% augite, with trace whitlockite and ilmenite. The clast is partly brecciated, primarily along grain boundaries, but it preserves much of its original adcumulate texture. Large cumulus plagioclase grains, up to 1.5 \times 0.8 mm in size, are separated in places by tiny post-cumulus augite grains (<100 μm across) and finer grains of ilmenite. Augite and ilmenite also form tiny inclusions in plagioclase. Shervais et al. (1984) reported pyroxene equilibration temperatures of 950 to 1050 $^{\circ}\text{C}$, which suggests that this sample formed in a shallow magma chamber that cooled relatively quickly (Shervais and McGee 1998b). A single, rounded inclusion (~50 μm across) of whitlockite occurs in plagioclase.

Ten spots were analyzed in this sample: two cores (one half-way to rim) and two rims in the largest cumulus plagioclase, two additional core-rim pairs in other cumulus plagioclase grains, an additional cumulus plagioclase core (adjacent to the rounded whitlockite inclusion), and one post-cumulus augite (Table 3).

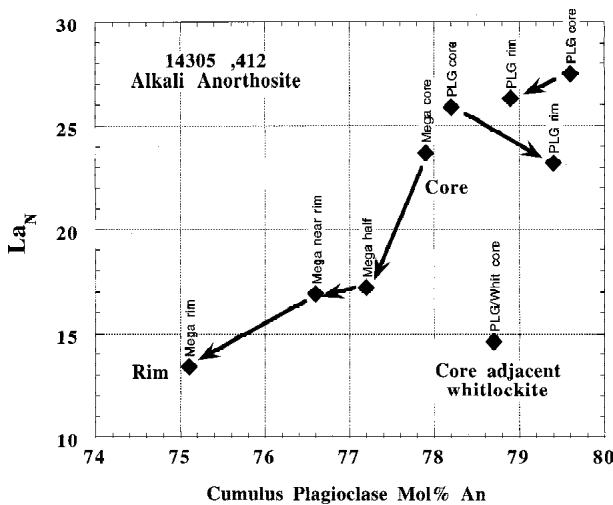


FIGURE 4. Correlation between plagioclase An content and La concentration in 14305,412. Core-Rim zoning traverses in large cumulus plagioclase grains.

All of the plagioclase spots are similar in composition, with La \sim 13–27 \times (Fig. 2g). The post-cumulus augite has a flat REE pattern at \sim 100 \times chondrite (Fig. 2g). There is a crude correlation between plagioclase An content and La content (Fig. 4).

DISCUSSION

Evaluation of post-cumulus reequilibration

Before we can invert the SIMS data to estimate the REE content of the alkali suite parental magma, we need to determine the nature and extent of any post-cumulus or subsolidus reequilibration. For the inversion process to be successful, cumulus mineral cores must preserve, or be close to, their original magmatic compositions. Papike et al. (1996) reported small differences between the ratio of distribution coefficients for pigeonite and plagioclase and the observed concentration ratios in magnesian-suite norites, which they suggested might result from reequilibration, with LREE diffusing into plagioclase and HREE diffusing into pigeonite during slow subsolidus cooling. Alternatively, these differences might reflect uncertainties in the experimental partition coefficients. Papike et al. concluded, however, that the amount of reequilibration is small and does not significantly affect the calculation of equilibrium parental magmas.

Several lines of evidence suggest that, for most of the cumulus plagioclase cores, the REE concentrations reported here result from primary igneous processes. Plagioclase rim analyses show the effect of interaction with late-stage intercumulus melt, but the difference in composition between the cumulus cores and rims is minor. Subsidiary reequilibration was important in only one sample (14304,279). The evidence for these conclusions is presented below.

First, five of the seven samples studied here are anorthosites that consist of \sim 95–99.5% plagioclase. Unlike the magnesian-suite norites studied by Papike et al. (1996), which contain subequal proportions of pyroxene and plagioclase, the alkali-

suite anorthosites do not contain a sink for the HREE or a source of LREE. One sample does contain accessory whitlockite (14305,412), but this occurs as a solitary inclusion in a cumulus plagioclase that has the same REE content as adjacent grains; as an inclusion, this whitlockite would make little contribution outside of its host phase.

Second, samples that have not been brecciated extensively and that preserve their primary textural relationships show core to rim variations in their trace element chemistry that are consistent with post-cumulus crystallization processes and that have not been homogenized by annealing (Fig. 4). The decrease in REE from core to rim in these samples implies saturation with an REE-rich phase in the trapped intercumulus liquid; similar trends have been observed by Jolliff and Floss (1997) in an alkali quartz monzogabbro. One sample, 14305,303, preserves extensive core-rim zoning of the major elements that has not been destroyed by annealing (Fig. 3). We discuss the significance of this sample further below.

Finally, four of the seven samples studied here have pyroxene equilibration temperatures of \sim 900–1050 °C (Fig. 5), based on the pyroxene thermometer of Lindsley and Anderson (1983). The high pyroxene equilibration temperatures show that these samples cooled too quickly for extensive subsolidus reequilibration, suggesting that they formed in shallow intrusions. This is supported by the lack of prominent exsolution features in the pyroxenes. Two other samples have pyroxene equilibration temperatures of \sim 700–800 °C, which implies slow cooling below the solidus (Fig. 5). However, both of these slowly cooled samples are also pure anorthosites, with $>$ 99% modal plagioclase (12033,575 and 12073,118). These samples have no source or sink for REE redistribution. Annealing of these samples could eliminate any core-rim variations, but the volume of core material in the primocrysts is much greater than the volume of post-cumulus rim material, and the core composition therefore should have undergone little change.

Only one of the samples studied here is a norite that contains both cumulus pyroxene and plagioclase (14304,279). The pyroxene in this sample is largely hypersthene that formed from inversion of pigeonite; augite occurs as exsolution lamellae in hypersthene and as late-crystallizing mantles on low-Ca py-

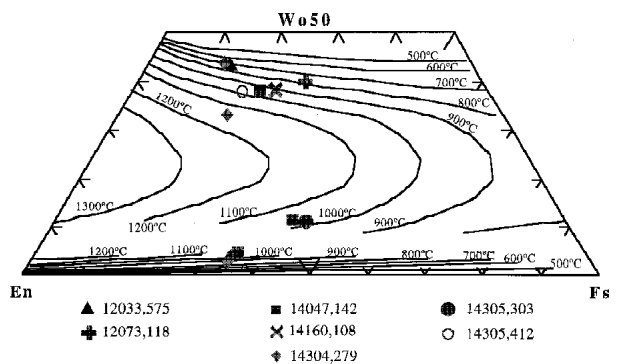


FIGURE 5. Equilibrium pyroxene temperatures for the samples studied here, using the pyroxene quadrilateral thermometer of Lindsley and Anderson (1983).

roxene. Equilibration temperatures for the hypersthene are about ~900–1000 °C (Fig. 5), close to the minimum stability temperature for coexisting pigeonite of ~1000–1050 °C (Lindsley and Anderson 1983). Augite temperatures vary from ~1100 °C (for cores of discrete grains) to ~700 °C (rims of same grains; Fig. 5). The high minimum stability temperature for the original pigeonite, the high calculated pyroxene temperatures for the resulting hypersthene and most augites, and the preservation of mesostasis glass all show that pigeonite inversion occurred above the basalt solidus (i.e., the sample was still saturated with interstitial melt, now represented by glass), and that subsequent cooling was relatively rapid.

A comparison of the concentration ratios in 14304,279 hypersthene and plagioclase to the ratio of low-Ca pyroxene/plagioclase distribution coefficients shows that the concentration ratios are equal to or higher than the ratio of distribution coefficients (Fig. 6). James et al. (1998) suggested that this relationship reflects supersolidus unmixing of augite from pigeonite and subsequent inversion of pigeonite to hypersthene, not igneous crystal/melt equilibria. As a result, the pyroxenes in this sample cannot be used to calculate the equilibrium parental-magma composition.

Core-rim zoning in 14305,412

The large number of points analyzed in anorthosite 14305,412, and its preservation of textural relationships, allow us to evaluate the effects of core-rim zoning. All of the plagioclase cores are characterized by La concentrations that are higher than their respective rims, but some core-rim pairs are higher in La than the cores and rims of other grains. There is also a crude correlation between plagioclase An content and La concentration in this sample (Fig. 4). Because there is no abundant sink for REE in this sample outside of the plagioclase, we interpret these variations to reflect primary igneous zonation of the cumulus plagioclase, equilibrating with an intercumulus melt phase that was lower in REE concentration than the primocryst-bearing parental magma. Similar trends

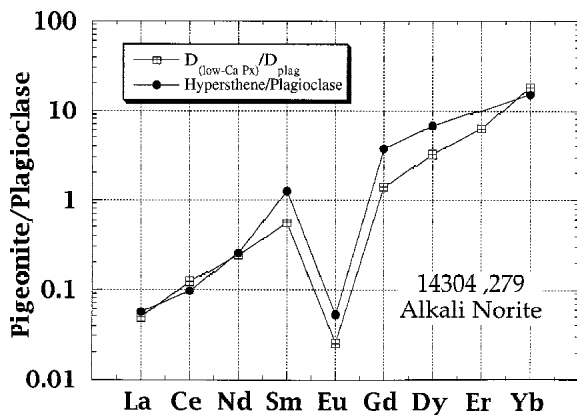


FIGURE 6. Comparison of concentration ratios hypersthene/plagioclase in sample 14304,279 to the ratio of distribution coefficients $D_{\text{low-Ca px}}/D_{\text{plag}}$ for the REE.

TABLE 4. Equilibrium distribution coefficients used in this study

Phase	High-Ca Pyroxene	Low-Ca Pyroxene	PLAG
La	0.07	0.002	0.041
Ce	0.1	0.004	0.033
Nd	0.21	0.006	0.025
Sm	0.26	0.011	0.020
Eu	0.31	0.006	1.150
Gd	0.3	0.021	0.015
Dy	0.33	0.032	0.010
Er	0.3	0.05	0.008
Yb	0.3	0.09	0.005

Sources: Pyroxenes = Grutzeck et al. 1974; Hack et al. 1994, McKay 1982, 1986, 1989; McKay et al. 1991; Nielsen et al. 1992; Plagioclase = Phinney and Morrison 1990; Phinney 1991.

have been documented by Jolliff and Floss (1997) for both plagioclase and pigeonite in quartz monzogabbro 14161,7373. We concur with the conclusion of Jolliff and Floss (1997) that whitlockite saturation in the intercumulus melt caused a decrease in REE concentrations of late-crystallizing rim assemblages. This is supported by the low La content of the cumulus plagioclase that contains the whitlockite inclusion (Fig. 4). An alternate explanation for the correlation between plagioclase An and La concentration is that REE substitution in plagioclase is controlled by crystal chemical effects, as suggested by Blundy and Wood (1991) for the elements Sr and Ba in plagioclase. Data presented by Bindeman et al. (1998) support the importance of crystal chemical controls on REE partitioning in plagioclase, but indicate that in general partition coefficients increase with decreasing An in plagioclase—the opposite of the behavior required to explain the positive correlation of La and An observed here.

Calculation of equilibrium magma compositions

Melts in equilibrium with the cumulus and post-cumulus phases were calculated using experimental and empirical partition coefficients for pyroxene and plagioclase (Grutzeck et al. 1974; McKay 1982, 1986, 1989; McKay et al. 1991; Phinney

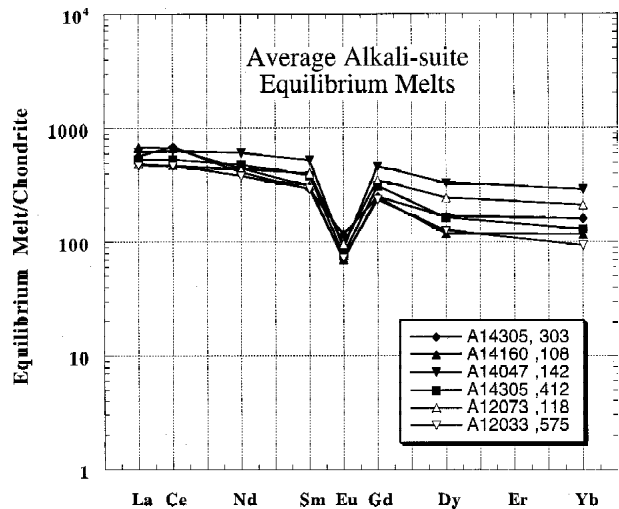


FIGURE 7. Calculated equilibrium magmas, normalized to chondritic meteorite, for average plagioclase cores in 12033,575; 12073,118; 14047,142; 14160,108; 14305,303; 14305,412.

TABLE 5. Average equilibrium parental magmas for Apollo 14 alkali-suite rocks studied here, normalized to chondrites

Equilibrium Liquids/Chondrite	KREEP	Average of All Alkali-suite	14305,303	14160,108	14160,108	14047,142	14305,412	12073,118	12033,575
La	324	558	567	678	251	614	531	490	469
Ce	297	575	686	663	317	631	532	471	469
Nd	310	457	408	440	287	605	476	432	381
Sm	251	366	290	308	284	526	382	401	290
Eu	41	86	115	70	25	87	77	96	72
Gd	240	308	249	245	271	460	309	348	235
Dy	228	191	167	118	269	329	162	243	126
Er	205				223				
Yb	180	166	160	116	270	286	131	211	93

and Morrison 1990; Phinney 1991; Nielsen et al. 1992; Hack et al. 1994; Jones 1995). The partition coefficients used in this study are listed in Table 4.

Six of the seven samples studied here appear to preserve primary igneous compositions (12033,575; 12073,118; 14047,142; 14160,108; 14305,303; 14305,412). Plagioclase core compositions reflect the composition of the equilibrium magma during crystallization of the only cumulate phase in these rocks. Plagioclase rim compositions reflect crystallization of the late intercumulus liquid, which was slightly depleted in REE relative to the original parental magma. Zoning in most cumulus plagioclase is minimal. This is consistent with cumulate theory, which holds that formation of nearly monomineralic cumulates requires that the inter-cumulus liquid remain in equilibrium with the main parental magma body (e.g., Wager and Brown 1960). Post-cumulus pyroxenes form after communication with the main parental magma ceases, and closed-system fractionation begins.

Equilibrium parental magmas calculated using primary cumulus plagioclase cores have La \sim 450–700 \times and Yb \sim 100–300 \times chondrite (Table 5, Fig. 7). Plagioclase rim compositions yield similar calculated equilibrium magmas, consistent with those calculated for the primary cumulus plagioclase cores. Although the calculated equilibrium magmas are broadly similar to the high-K KREEP component of Warren (1989), they have some significant differences. First, all of the calculated equilibrium magmas are depleted in the HREE and enriched in LREE relative to KREEP (Fig. 8). Average parental magmas based on selected core compositions have La concentrations \sim 1.5–2.0 \times high-K KREEP, but their Yb concentrations are only \sim 0.6–1.6 \times high-K KREEP (Fig. 8). Second, almost all of the calculated parental magmas have small positive Eu anomalies relative to KREEP (Fig. 8). This is consistent with whole-rock geochemical data, which show that all western alkali anorthosites have higher Eu than associated magnesian-suite anorthosites, troctolites, and norites (Warren et al. 1983a). Both of these effects are consistent with the assimilation of plagioclase into a KREEP-like parental magma (e.g., Shervais and McGee 1998b, 1998c), as argued below.

Alkali anorthosites: Flotation cumulates from a KREEP basalt parental magma

Equilibrium parental magmas for the alkali-suite cumulates studied here, calculated using SIMS analyses of cumulus plagioclase cores, all have REE concentrations \sim 0.6–2.0 \times high-K KREEP (Fig. 8). These data are consistent with the proposal of

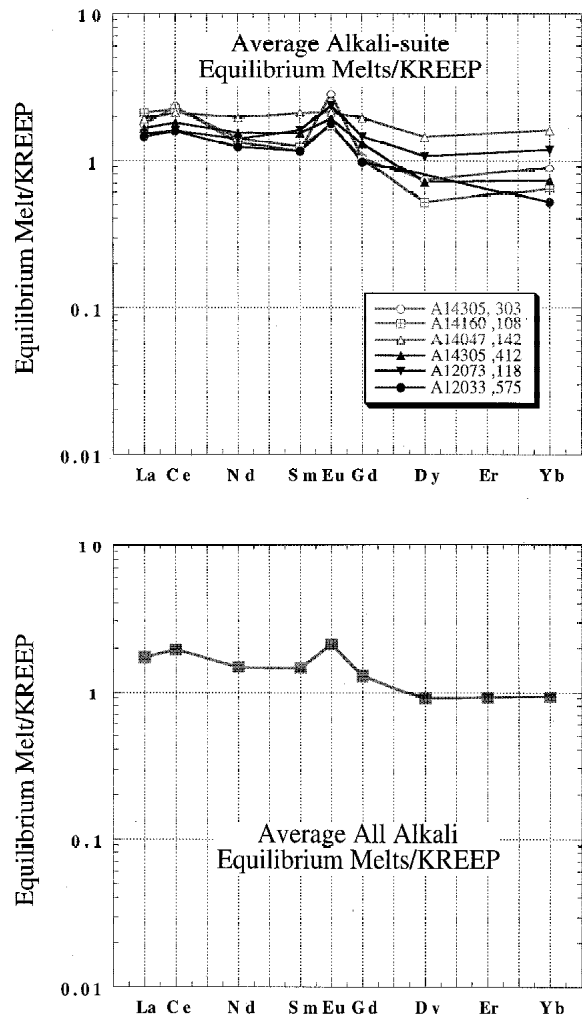


FIGURE 8. Calculated equilibrium parental magmas, normalized to the high-K KREEP of Warren (1989). (a) For average plagioclase cores in 12033,575; 12073,118; 14047,142; 14160,108; 14305,303; 14305,412. (b) Average of all alkali suite equilibrium parental magmas, normalized to the high-K KREEP.

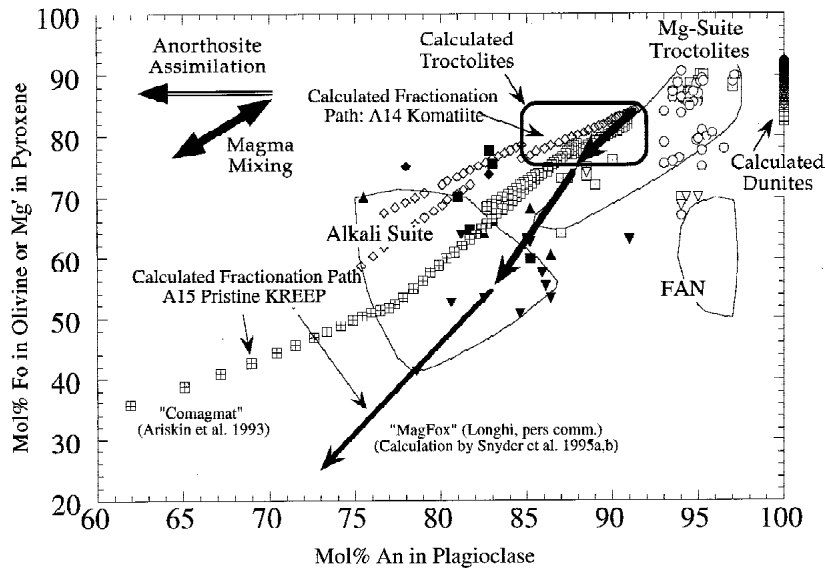


FIGURE 9. Fo-An diagram for all pristine plutonic rocks of the western lunar highlands, showing calculated fractionation paths for crystal extracts from the average Apollo 15 pristine KREEP basalt from Snyder et al. (1995), using the MAGFOX program of Longhi (1980, 1991). Path calculated here with the COMAGMAT software of Ariskin et al. (1993) shown with open boxes (olivine, olivine+plagioclase) and open diamonds (pyroxene+plagioclase). Path calculated by Snyder et al. (1995) shown with bold arrows: thickest = olivine+plagioclase, medium thick = pigeonite+plagioclase, thin = pigeonite/augite/fayalite+plagioclase. Other symbols show Apollo 12 and 14 pristine rocks. Magnesian suite: ○ = olivine-plagioclase, □ = Opx-plagioclase, ▽ = Pigeonite-plagioclase. Alkali suite: ◆ = olivine-plagioclase, ■ = Opx-plagioclase, ▼ = pigeonite-plagioclase, ▲ = augite-plagioclase.

Snyder et al. (1995a) that cumulate rocks of the alkali suite crystallized from a parental magma similar in composition to the Apollo 15 pristine KREEP basalts. Several lines of evidence suggest that anorthositic rocks of this suite formed as flotation cumulates in compositionally zoned, shallow magma chambers, perhaps in concert with more mafic cumulates of the magnesian suite gabbronorites.

Anorthosite and anorthositic norite are the most common rocks of the alkali suite. Forward modeling of a typical Apollo 15 pristine KREEP basalt composition using the melt equilibria program COMAGMAT (Ariskin et al. 1993) shows that phase compositions characteristic of the alkali suite are formed after about 40 mol% crystallization (Fig. 9); Snyder et al. (1995a) reached the same conclusion using the the MAGFOX program of Longhi (1980, 1991). The cotectic phase proportions in this interval are ~35–40 mol% plagioclase and ~65–60 mol% pyroxene (augite and/or pigeonite). These proportions are only observed in one rock studied here (14304,279), which thus may have formed by cotectic equilibrium crystallization of a pristine KREEP-like magma. All of the other samples studied here, and a majority of alkali-suite samples in general (e.g., Warren 1993), contain >85% modal plagioclase. Flotation of plagioclase in a shallow magma chamber is a plausible and efficient way to effect this concentration of plagioclase (e.g., Morse 1968), but anorthosite assimilation is another mechanism that may form alkali anorthosites (Shervais and McGee 1998b; see below).

The high pyroxene equilibration temperatures calculated for five of the seven plutonic rocks studied here (Fig. 5) and the lack of exsolution textures in four of these same samples re-

quire that they cooled relatively quickly and thus probably formed in shallow magma chambers. Accumulation of plagioclase by flotation near the roof (where heat loss is greatest) would enhance cooling. In contrast, many plutonic rocks of the magnesian suite have annealed textures and pyroxenes with low equilibration temperatures, consistent with slow cooling in relatively deep magma chambers (e.g., James 1980; but also see McCallum and O'Brien 1996). Some magnesian-suite cumulates also contain olivine and plagioclase in near cotectic proportions, consistent with the gravitational accumulation of both phases.

Anorthosite assimilation: A forcing mechanism for sodic plagioclase crystallization

Calculated equilibrium liquids for the six samples that we infer to preserve primary igneous partitioning all have small positive Eu anomalies, and are enriched in LREE, relative to high-K KREEP (Fig. 8). We suggest that these anomalies result from the assimilation of older, pre-existing anorthosites during the course of alkali suite crystallization (Shervais and McGee 1998b). In addition to increasing the LREE and Eu content of the magma, this assimilation would move the bulk composition of the system towards anorthite, thus forcing increased crystallization of plagioclase. The composition of the equilibrium plagioclase would not become more calcic, however, because the system could not increase in temperature. The added calcic plagioclase would dissolve into the melt (which is undersaturated in plagioclase of that composition), balanced by crystallization of more equilibrium plagioclase (Tsuchiyama

1985a, 1985b). As a result, assimilation of calcic plagioclase would force the crystallization of additional plagioclase with a more-sodic composition and lower the proportion of melt remaining (e.g., Morse 1980).

This effect is even more pronounced in the diopside-saturated ternary system (Plag-Di-Liq), where assimilation would force the liquid composition off the cotectic into the plagioclase-only volume along an isotherm. Because isotherms in the plagioclase volume of the Di-An-Ab system slope toward albite, the resulting contaminated liquid compositions would become more sodic (J.H. Longhi, personal communication 1998). The calcic plagioclase assimilant would dissolve because the melt is undersaturated with plagioclase of that composition (Tsuchiyama 1985a, 1985b). Dissolution of the calcic plagioclase would be compensated by the crystallization of additional plagioclase with a more-sodic composition that is in equilibrium with the new melt composition (Tsuchiyama 1985a, 1985b). This reaction uses up large quantities of liquid and greatly increases the proportion of crystals-to-liquid.

On Earth, assimilation typically occurs through syntexis (e.g., Brammall 1933; Dobretsov and Marin 1986; Bédard and Hébert 1996). Syntexis is the process of assimilation that includes stoping of roof rocks into the magma chamber and their physical disaggregation in response to partial melting. The physical disaggregation of stoped blocks increases the surface area exposed to the host magma and promotes further melting and disaggregation. This process is common in many terrestrial plutons and is expected to be important on the Moon also. Objections to anorthosite assimilation based on thermal considerations (e.g., Finnilla et al. 1994) are flawed because they use a physically improbable model for magma-rock interaction (the flat upper surface of a horizontal, sill-like intrusion with no thermal convection). Models that involve syntexis are more realistic physically and result in thermal regimes similar to those found during vigorous thermal convection. A further point here is that syntexis and assimilation have only a small effect on magma composition, but a significant effect on both the proportions and compositions of the resulting crystals. Assimilation is not an effective way to alter the composition of large quantities of melt (i.e., to create an extensive liquid line-of-descent) because the composition of the liquid is not strongly affected and because large volumes of melt are used by the plagioclase-forming reaction. In contrast, assimilation results in large volumes of equilibrium plagioclase with compositions that are more sodic than the calcic plagioclase assimilant.

Magma mixing and the origin of reversed zoning in plagioclase

The complex reverse zoning observed in sample 14305,303 (Fig. 3) cannot result from assimilation of more calcic plagioclase. As noted above, this process will force the crystallization of additional amounts of a more-sodic plagioclase that is similar in composition to the equilibrium plagioclase prior to assimilation. In the absence of high water vapor pressures on the moon, the reverse zoning observed in 14305,303 could only form by the mixing of a hotter, more primitive magma with an evolved magma that already contained the $\sim\text{An}_{84}$ cores (Shervais and McGee 1998c). The resulting mixed magma was in equilibrium with An_{91} plagioclase,

which formed thick mantles on the more sodic cores, until closed-system crystallization led to renewed zoning toward $\sim\text{An}_{87}$ rims (Fig. 3). Tsuchiyama (1985a, 1985b) has shown that immersion of sodic plagioclase in a diopside-saturated melt that is in equilibrium with a more-calcic plagioclase will cause partial dissolution of the disequilibrium sodic feldspar, followed by crystallization of more-calcic equilibrium feldspar that forms a mantle on the partly resorbed core. The textures produced experimentally by Tsuchiyama (1985a) are directly analogous to those observed in alkali anorthosite 14305,303.

Based on our calculations with COMAGMAT and a pristine KREEP basalt parent, the An_{91} mantles seen in 14305,303 are similar to the most-calcic plagioclase to form from this magma composition (Fig. 9). If we assume that a magma similar in major-element composition to pristine KREEP basalt is an appropriate parental magma composition for the alkali-suite cumulates, the An_{91} mantles on the large cumulus plagioclase grains in 14305,303 imply a nearly complete replenishment of the magma chamber with primitive melt. This seems to require the injection of new primitive melt into the system, but it may occur by convective overturn in a compositionally zoned (and gravitationally unstable) magma chamber.

IMPLICATIONS FOR LUNAR PETROGENESIS

The data presented here suggest that alkali-suite anorthosites preserve major and trace element characteristics acquired during their formation as igneous cumulate rocks, and that these characteristics can be used to reconstruct the equilibrium parental magma composition. Our data show that cumulates of the alkali suite crystallized from magmas with REE contents $\sim 0.6\text{--}2.0\times$ high-K KREEP. As proposed by Snyder et al. (1995a), the alkali-suite parental magma may be similar in major-element composition to Apollo 15 pristine KREEP basalt. If so, this magma was modified by anorthosite assimilation to force the crystallization of additional sodic plagioclase, which formed flotation cumulates near the roof of shallow, compositionally zoned magma chambers. Convective overturn of this magma chamber (possibly induced by the injection of new primitive melt) occurred episodically, as shown by reverse zoning profiles in some cumulus plagioclase.

ACKNOWLEDGMENTS

The SIMS analyses reported in this paper were performed at the Woods Hole Oceanographic Institute/MIT SIMS Facility, under the direction of Nobu Shimizu, with assistance from N. Shimizu and P. Kelemen. This work was supported by NASA grants NAG9-169 and NAGW-3637. J. Stuart assisted with the microprobe analyses of 14305,303, supported by an undergraduate research fellowship from the South Carolina Space Grant Consortium. We also thank Carleton Moore for access to a sample of Moore County meteorite. Conversations with N. Shimizu, P. Kelemen, G. Layne, C. Shearer, O. James, J. Longhi, and B. Jolliff about SIMS analyses and lunar petrology helped us think more clearly. Thorough reviews by C. Shearer and G. Snyder were very helpful for improving the manuscripts.

REFERENCES CITED

- Ariskin, A.A., Frenkel, M.Y., Barmina, G.S., and Nielsen, R.L. (1993) Comagmat: A Fortran program to model magma differentiation processes. *Computers and Geosciences*, 19, 1155–1170.
- Bédard, J.H. and Hébert, R. (1996) The lower crust of the Bay of Islands ophiolite, Canada: Petrology, mineralogy, and the importance of syntexis in magmatic differentiation of ophiolites and at ocean ridges. *Journal of Geophysical Research*, 101, B11, 25105–25124.
- Bindeman, I.N., Davis, A.M., and Drake, M.J. (1998) Ion microprobe study of plagioclase-basalt partition experiments at natural concentration levels of trace el-

- ements. *Geochimica Cosmochimica Acta*, 62, No. 7, 1175–1193.
- Blundy, J.D. and Wood, B.J. (1991) Crystal-chemical control on the partitioning of Sr and Ba between plagioclase feldspar, silicate melts, and hydrothermal solutions. *Geochimica Cosmochimica Acta*, 55, 193–209.
- Brammal, A. (1933) Syntexis and differentiation. *Geological Magazine*, 70, 97–107.
- Crozaz, G. and Zinner, E. (1985) Ion probe determinations of the REE concentrations of individual meteorite phosphate grains. *Earth and Planetary Science Letters*, 73, 41–52.
- Dobretsov, G.L. and Marin, Y.B. (1986) Syntexis and its petrogenetic role. *International Geology Review*, 28, 875–885.
- Finnila, A.B., Hess, P.C., and Rutherford, M.J. (1994) Assimilation by lunar mare basalts: melting of crustal material and dissolution of anorthite. *Journal of Geophysical Research Supplement*, 99, E7, 14677–14690.
- Galbraith, K.C., Shearer, C.K., Papike, J.J., and Shimizu, N. (1990) Inter- and intra-group compositional variations in Apollo 15 pyroclastic green glass: An electron and ion microprobe study. *Geochimica Cosmochimica Acta*, 54, 2565–2575.
- Goodrich, C.A., Taylor, G.J., Keil, K., Kallemeyn, G.W., and Warren, P.H. (1986) Alkali norite, troctolites, and VHK mare basalts from breccia 14304. *Proceedings of the Lunar and Planetary Science Conference 16th*, *Journal of Geophysical Research*, 91, D305–D318.
- Grutzeck, M., Kridelbaugh, S., and Weill, D. (1974) The distribution of Sr and REE between diopside and silicate liquid. *Geophysical Research Letters*, 1, 273–275.
- Hack, P.J., Nielsen, R.L., and Johnston, A.D. (1994) Experimentally determined rare-earth element and Y partitioning behavior between clinopyroxene and basaltic liquids at pressures up to 20kbar. *Chemical Geology*, 117, 89–105.
- James, O.B. (1980) Rocks of the early lunar crust. *Proceedings of the Lunar and Planetary Science Conference 11th*, *Geochimica Cosmochimica Acta*, Supplement 12, Volume 1, 365–393.
- James, O.B., Floss, C., and McGee, J. J. (1998) Rare-earth distributions in pyroxenes from a lunar mafic-magnesian ferroan anorthosite (CD ROM format). In *Lunar and Planetary Science XXIX*, Abstract no. 1292, Lunar and Planetary Institute, Houston, Texas.
- Jolliff, B.L. and Floss, C. (1997) Liquid immiscibility in a lunar plutonic setting and the evolution of KREEPy residual melts. *Lunar and Planetary Science XXVIII*, Lunar and Planet Institute, Houston.
- Jolliff, B.L., Haskin, L.A., Colson, R., and Wadhwa, M. (1993) Partitioning in REE-saturated minerals: Theory, experiments, and modelling of whitlockite, apatite, and evolution of lunar residual magmas. *Geochimica Cosmochimica Acta*, 57, 4069–4094.
- Jones, J.H. (1995) Experimental trace element partitioning, in *Rock Physics and Phase Relations. A Handbook of Physical Constants*, American Geophysical Union Shelf Reference, 3, 83.
- Lindsley, D.H. and Anderson, D.J. (1983) A two-pyroxene thermometer. *Journal of Geophysical Research*, 88, A887–A906.
- Longhi, J. (1980) A model of early lunar differentiation. *Proceedings of the Lunar and Planetary Science Conference 11th*, *Geochimica Cosmochimica Acta*, Supplement 12, 289–315.
- (1991) Comparative liquidus equilibria of hypersthene normative basalts at low pressures. *American Mineralogist*, 76, 785–800.
- McCallum, I.S. and O'Brien, H.E. (1996) Stratigraphy of the lunar highland crust: Depths of burial of lunar samples from cooling rate studies. *American Mineralogist*, 81, 1166–1175.
- McKay, G.A. (1982) Partitioning of REE between olivine, plagioclase, and synthetic basalt melts: implications for the origin of lunar anorthosites. *Lunar and Planetary Science XIII*, Lunar and Planetary Institute, Houston, 493–494.
- (1986) Crystal/liquid partitioning of REE in basaltic systems: extreme fractionation of REE in olivine. *Geochimica Cosmochimica Acta*, 50, 69–79.
- (1989) Partitioning of rare earth elements between major silicate minerals and basaltic melts. In *Mineralogical Society of America Reviews in Mineralogy*, 21, 45–78.
- McKay, G.A., Le, L., and Wagstaff, J. (1991) Constraints on the origin of mare basalt Eu anomaly: REE partition coefficients for pigeonite, *Lunar and Planetary Science XXII*, 883–884.
- Meyer, C., Brett, R., Hubbard, N.J., Morrison, D.A., McKay, D.S., Aitken, F.K., Takeda, H., and Schonfeld, E. (1971) Mineralogy, chemistry, and origin of the KREEP component in soil samples from the Ocean of Storms, *Proceedings of 2nd Lunar Science Conference*, *Geochimica Cosmochimica Acta*, Supplement 2, 1, 393–411.
- Morse, S.A. (1968) Layered intrusions and anorthosite genesis. In Y.W. Isachsen, Ed., *Origin of Anorthosite and Related Rocks*, Memoir 18, 175–188. New York State Museum and Science Service, Albany, New York.
- (1980) *Basalts and Phase Diagrams*, 342 p. Springer Verlag, New York.
- Nielsen, R.L., Gallahan, W.E., and Newberger, F. (1992) Experimentally determined mineral-melt partition coefficients for Sc, Y and REE for olivine, orthopyroxene, pigeonite, magnetite and ilmenite. *Mineralogy and Petrology*, 110, 488–499.
- Papike, J.J. (1996) Pyroxene as a recorder of cumulate formational processes in asteroids, Moon, Mars, Earth: Reading the record with the ion microprobe. *American Mineralogist*, 81, 525–544.
- Papike, J.J., Shearer, C.K., and Galbraith, K.C. (1990) Reading the volcanic record of the moon by ion microprobe analysis of lunar glass beads. *Geology*, 18, 295–298.
- Papike, J.J., Fowler, G.W., Shearer, C.K. (1994) Orthopyroxene as a recorder of lunar Mg-suite norite petrogenesis: an ion microprobe investigation of Mg suite norites. *American Mineralogist*, 79, 796–800.
- Papike, J.J., Fowler, G.W., Shearer, C.K., and Layne, G.D. (1996) Ion Microprobe investigation of plagioclase and orthopyroxene from lunar Mg-suite norites: Implications for calculating parental melt REE concentrations and for assessing postcrystallization REE redistribution. *Geochimica Cosmochimica Acta*, 60, 3967–3978.
- Phinney, W.C. (1991) Lunar anorthosites, their equilibrium melts, the bulk moon. *Proceedings of Lunar and Planetary Science 21st*, Lunar and Planetary Institute, Houston, 29–49.
- Phinney, W.C. and Morrison, D.A. (1990) Partition coefficients for calcic plagioclase: implications for Archean anorthosites. *Geochimica Cosmochimica Acta*, 54, 1639–1654.
- Pouchou, J.L. and Pichoir, F. (1991) Quantitative analysis of homogeneous or stratified microvolumes applying the model “PAP”. In K.F.J. Heinrich and D.E. Newbury, Eds., *Electron Probe Quantitation*, 31–76. Plenum Press, New York.
- Roden, M.F. and Shimizu, N. (1993) Ion microprobe analyses bearing on the composition of the upper mantle beneath the basin and range and Colorado plateau provinces. *Journal of Geophysical Research*, 98/B8, 14091–14108.
- Shearer, C.K., Papike, J.J., Simon, S.B., Shimizu, N., Yurimoto, H., and Sueno, S. (1990) Ion microprobe studies of trace elements in Apollo 14 volcanic glass beads: comparisons to Apollo 14 mare basalts and petrogenesis of picritic melts. *Geochimica Cosmochimica Acta*, 54, 851–867.
- Shervais, J.W. (1989) Highland Crust at the Apollo 14 Site: A Review. In G.J. Taylor and P.H. Warren, Eds., *Workshop on Moon in Transition: Apollo 14, KREEP, and Evolved Lunar Rocks*, LPI Technical Report 89–03, p. 118–127. Lunar and Planetary Institute, Houston, Texas.
- (1994) Ion Microprobe Studies of Lunar Highland Cumulate Rocks: Preliminary Results, 1265–1266. *Lunar and Planetary Science XXV*, Lunar and Planetary Institute, Houston, Texas.
- (1996) Ion Microprobe Study Of Lunar Cumulate Rocks From The Apollo 12 and 14 Sites: Evidence for the Involvement Of KREEP In Alkali Suite And Mg-Rich Suite Parent Magmas. *Geological Society of America, Abstracts with Programs*, Denver.
- Shervais, J.W. and McGee, J.J. (1997a) KREEP in the lunar highlands: Ion Microprobe Studies of Lunar Highland Cumulate Rocks, p. 1285–1286. *Lunar and Planetary Science XXVIII*, Lunar and Planetary Institute, Houston, Texas.
- (1997b) Petrogenesis of alkali suite anorthosites and norites in the western lunar highlands: flotation cumulates from pristine KREEP, magma-mixing, and assimilation of older anorthosites. *Meteoritics and Planetary Science*, 32, A119.
- (1998a) Ion & Electron microprobe study of Troctolites, Norite, and Anorthosites from Apollo 14: Evidence for urKREEP Assimilation during petrogenesis of Apollo 14 Mg-Suite Rocks. *Geochimica Cosmochimica Acta*, Volume 62, No. 17, 3009–3023.
- (1998b) Alkali suite anorthosites and norites: Flotation cumulates from pristine KREEP with magma mixing and the assimilation of older anorthosite (CD-ROM format). In *Lunar and Planetary Science XXIX*, Abstract no. 1699, Lunar and Planetary Institute, Houston, Texas.
- (1998c) Magma mixing in the petrogenesis alkali suite anorthosites: reverse zoning in plagioclase, 14305.303 (CD-ROM format). In *Lunar and Planetary Science XXIX*, Abstract no. 1706, Lunar and Planetary Institute, Houston, Texas.
- Shervais, J.W. and Stuart, J.B. (1995) Ion Microprobe Studies of Lunar Highland Cumulate Rocks: New Results, p. 1285–1286. *Lunar and Planetary Science XXVI*, Lunar and Planetary Institute, Houston, Texas.
- Shervais, J.W., Taylor, L.A., Lail, J.C., and Smith, M.R. (1984) Pristine highland clasts in consortium breccia 14305: Petrology and geochemistry. *Proceedings of the Lunar and Planetary Science Conference 15th*. *Journal of Geophysical Research*, 89, C25–C40.
- Shervais, J.W., Vetter, S.K., and Lindstrom, M.M. (1990) Chemical differences between small subsamples of Apollo 15 olivine-normative basalts. *Proceedings of the 20th Lunar and Planetary Science Conference*, Lunar and Planetary Institute, Houston, 109–126.
- Shimizu, N. (1978) Analyses of zoned plagioclase of different magmatic environments: a preliminary ion microprobe study, *Earth and Planetary Science Letters*, 39, 395–406.
- (1997) Principles of SIMS and modern ion microprobes. In R. Gill, Ed., *Modern Analytical Geochemistry*, p. 235–242. Addison-Wesley Longman, New York.
- Shimizu, N. and Hart, S.R. (1982) Applications of the ion microprobe to geochemistry and cosmochemistry, *Annual Reviews of Earth and Planetary Science*, 10, 483–526.
- Snyder, G.A., Taylor, L.A., Liu, Y-G., and Schmitt, R.A. (1992) Petrogenesis of the western highlands of the Moon: Evidence from a diverse group of whitlockite-rich rocks from the Fra Mauro Formation. *Proceedings of Lunar and Planetary Science*, 22, Lunar and Planetary Institute, Houston, 339–416.
- Snyder, G.A., Taylor, L.A., and Crozaz, G. (1993) Rare earth element selenochemistry of immiscible liquids and zircon at Apollo 14: an ion microprobe study of evolved rocks on the moon. *Geochimica Cosmochimica Acta*, 57, 1143–1149.
- Snyder, G.A., Neal, C.R., Taylor, L.A., and Halliday, A.N. (1994) Petrology and chemistry of the magnesian suite: further evidence of liquid immiscibility and

- metasomatism in the western lunar highlands. *Lunar and Planetary Science XXV*, Lunar and Planetary Institute, Houston, 1305–1306.
- Snyder, G.A., Taylor, L.A., Jerde, E.A., and Halliday, A.N. (1995a) Chronology and petrogenesis of the lunar highlands alkali suite: cumulates of KREEP basalt crystallization. *Geochimica Cosmochimica Acta*, 59, 1185–1203.
- Snyder, G.A., Neal, C.R., Taylor, L.A., and Halliday, A.N. (1995b) Processes involved in the formation of magnesian-suite plutonic rocks from the highlands of the Earth's Moon. *Journal of Geophysical Research*, 100, E5, 9365–9388.
- Tschiyama, A. (1985a) Dissolution kinetics of plagioclase in the melt of the system diopside-albite-anorthite, and the origin of dusty plagioclase in andesites. *Contributions to Mineralogy and Petrology*, 89, 1–16.
- (1985b) Partial melting kinetics of plagioclase-dioside pairs. *Contributions to Mineralogy and Petrology*, 91, 12–23.
- Wager, L.R. and Brown, G.M. (1960) *Layered igneous rocks*, 588 p. W.H. Freeman and Company, San Francisco.
- Warren, P.H. (1988) Origin of pristine KREEP: effects of mixing between urKREEP and magmas parental to the Mg-rich cumulates. *Proceedings of the 18th Lunar and Planetary Science Conference*. Lunar and Planetary Institute, Houston, 233–242.
- (1989) KREEP: Major element diversity, trace element uniformity (almost), in G.J. Taylor and P.H. Warren, Eds., *Workshop on Moon in Transition: Apollo 14, KREEP, and Evolved Lunar Rocks*, LPI Technical Report 89–03, p. 149–153. Lunar and Planetary Institute, Houston, Texas.
- (1993) A concise compilation of petrologic information on possibly pristine nonmare moon rocks. *American Mineralogist*, 78, 360–376.
- Warren, P.H. and Wasson, J.T. (1980) Further foraging for pristine nonmare rocks: correlations between geochemistry and longitude. *Proceedings of the Lunar Planetary Science Conference 11th*, *Geochimica Cosmochimica Acta*, Supplement 12, 431–470.
- Warren, P.H., Taylor, G.J., Keil, K., Marshall, C., Wasson, J.T. (1981) Foraging westward for pristine nonmare rocks: Complications for petrogenetic models. *Proceedings of the Lunar Planetary Science Conference 12th*, *Geochimica Cosmochimica Acta*, Supplement, 21–40.
- Warren, P.H., Taylor, G.J., Keil, K., Kallemeyn, G.W., Rosener, P.S., and Wasson, J.T. (1983a) Sixth foray for pristine nonmare rocks and an assessment of the diversity of lunar anorthosite. *Proceedings of the Lunar and Planetary Science Conference 13th*. *Journal of Geophysical Research*, 88, A615–A630.
- Warren, P.H., Taylor, G.J., Keil, K., Kallemeyn, G.W., Shirley, D., and Wasson, J.T. (1983b) Seventh foray: whitlockite-rich lithologies, a diopside bearing troctolitic anorthosite, ferroan anorthosites, and KREEP. *Proceedings of the 14th Lunar and Planetary Science Conference*. *Journal of Geophysical Research Supplement*, 88, A615–A630.
- Warren, P.H., Jerde, E.A., and Kallemeyn, G.W. (1990) Pristine moon rocks: an alkali anorthosite with coarse augite exsolution from plagioclase, a magnesian harzburgite, and other oddities, p. 31–59. *Proceedings 20th Lunar and Planetary Science Conference*, Lunar and Planetary Institute, Houston, Texas.

MANUSCRIPT RECEIVED JUNE 3, 1997

MANUSCRIPT ACCEPTED JANUARY 13, 1999

PAPER HANDLED BY BRAD L. JOLLIFF